Heliyon 10 (2024) e32419

Contents lists available at ScienceDirect

Heliyon

journal homepage: www.cell.com/heliyon

Research article

Crystallographic structure, antibacterial effect, and catalytic activities of fig extract mediated silver nanoparticles

Md Ohiduzzaman [a,b,**], M.N.I. Khan [c], K.A. Khan [a,d], Bithi Paul [e,*], Md Nazmul Hasan Zilani [f], Md Nazmul Hasan [g]

[a] Department of Physics, Jagannath University, Dhaka, 1100, Bangladesh
[b] Department of Physics, Jashore University of Science and Technology, Jashore, 7408, Bangladesh
[c] Materials Science Division, Atomic Energy Centre, Dhaka, Bangladesh
[d] Bangamata Sheikh Fojilatunnesa Mujib Science & Technology University, Jamalpur, Bangladesh
[e] Department of Physics, American International University-Bangladesh, Dhaka, Bangladesh
[f] Department of Pharmacy, Jashore University of Science and Technology, Jashore, 7408, Bangladesh
[g] Department of Genetic Engineering and Biotechnology, Jashore University of Science and Technology, Jashore, 7408, Bangladesh

ARTICLE INFO

Keywords:
Biosynthesis
Fig extract
Ag NPs
FE-Electrochemical cell
Antibacterial activity
Internal resistance
Voltage regulation

ABSTRACT

Silver nanoparticles (Ag NPs) play a pivotal role in the current research landscape due to their extensive applications in engineering, biotechnology, and industry. The aim is to use fig (*Ficus hispida* Linn. f.) extract (FE) for eco-friendly Ag NPs synthesis, followed by detailed characterization, antibacterial testing, and investigation of bioelectricity generation. This study focuses on the crystallographic features and nanostructures of Ag NPs synthesized from FE. Locally sourced fig was boiled in deionized water, cooled, and doubly filtered. A color change in 45 mL 0.005 M $AgNO_3$ and 5 mL FE after 40 min confirmed the bio-reduction of silver ions to Ag NPs. Acting as a reducing and capping agent, the fig extract ensures a green and sustainable process. Various analyses, including UV–vis absorption spectrophotometry (UV), X-ray diffraction (XRD), Fourier-transform infrared spectroscopy (FTIR), Field emission scanning electron microscopy (FESEM), Energy dispersive X-ray spectroscopy (EDX) and Transmission electron microscopy (TEM) were employed to characterize the synthesized nanoparticles, and Gas chromatography-mass spectrometry (GC-MS) analysis of the fig extract revealed the presence of eleven chemicals. Notably, the Ag NPs exhibited a surface plasmon resonance (SPR) band at 418 nm, confirmed by UV analysis, while FTIR and XRD results highlighted the presence of active functional groups in FE and the crystalline nature of Ag NPs respectively. With an average particle size of 44.57 nm determined by FESEM and a crystalline size of 35.87 nm determined by XRD, the nanoparticles showed strong antibacterial activities against *Staphylococcus epidermidis* and *Escherichia coli*. Most importantly, fig fruit extract has been used as the bio-electrolyte solution to generate electricity for the first time in this report. The findings of this report can be the headway of nano-biotechnology in medicinal and device applications.

* Corresponding author.
** Corresponding author. Department of Physics, Jagannath University, Dhaka, 1100, Bangladesh.
E-mail addresses: ohid@just.edu.bd (M. Ohiduzzaman), chyabithi@gmail.com (B. Paul).

https://doi.org/10.1016/j.heliyon.2024.e32419
Received 6 March 2024; Received in revised form 3 June 2024; Accepted 4 June 2024
Available online 4 June 2024

1. Introduction

Metal-based nanoparticles, notably Ag NPs, have captured significant scientific interest owing to their exceptional biological and physicochemical characteristics [1,2]. Compared to their bulk counterparts, Ag NPs display distinct properties like catalytic activity, high thermal and electrical conductivity, chemical stability, surface-enhanced Raman scattering, good redox activity, nonlinear optical behavior, and antimicrobial effects [3–5]. These attributes make them highly versatile and applicable in diverse fields such as cosmetics, shampoos, soaps, detergents, electronics, medicine, and more [6,7]. Moreover, their high surface-area-to-volume ratio allows for customization, enhancing their toxicity against pathogens, cancer cell eradication, and catalytic efficiency [8].

The application scope of nanomaterials, including metal nanoparticles like Ag, Au, CuO, ZnO, NiO, and MnO spans antibacterial, drug delivery, antifungal, and antioxidant functionalities [9,10,11–14]. Particularly, Au and Ag nanoparticles are extensively used in medical devices and hygiene products due to their superior antimicrobial, anti-inflammatory, and antifungal properties at the nanoscale, outperforming traditional drugs in efficacy [13,15].

The synthesis methods greatly impact the acceptability and utility of these nanoparticles in various applications [16]. Traditional chemical synthesis involving toxic organic solvents raises environmental and health concerns [17]. Consequently, there's a growing emphasis on biological techniques for nanoparticle production, promoting less expensive, non-toxic, high purity, and more environmentally benign processes [4,18,19]. Undoubtedly, there are many easy and fast conventional methods to synthesize the Ag NPs commercially but biosynthesis of Ag NPs by using verities plant extracts is the most favorable for the exploration of multiple antimicrobial activities such as antibacterial, antifungal, anticancer, antitumor, drug delivery, antidiabetic, and nanomedicine [6,8,16,20,21]. Even different bacteria and fungi have been used to synthesize the Ag NPs for clinical applications [21].

Beside the biological applications green synthesized Ag NPs have been used in photocatalytic, harvesting solar energy, and thin film applications for their tremendous optoelectronic properties [14,22,23,24,25]. The optical and antimicrobial properties of Ag NPs vary with the particle size and the desired particle size depends on the reaction temperature, concentration, and P^H of plant extract [26,27].

Till date, different plants extract have been utilized, including those from *Eucalyptus globulus* [28], *Hibiscus cannabinus* L [29], *Premna integrifolia* L. [30], *Lobelia rucotianifolia* [31], *Azadirachta indica (neem)* [32], *Murraya koenigii (Linn)* [33], *Rhamnus alaternus* [34], *Stevia redaudiana* [35], olive leaves [36], pure heart plant [37], *Terminalia arjuna* [38], *Artemisia oliveriana* [39], *Persicaria odorata* [40], *Acacia ehrenbergiana* Plant Cortex [41], *Citrus macroptera* fruit [42], Camellia sinensis L. [43], and *Paulownia fortunei* fruit [44] to optimize the optimum parameters to fabricating the desire sized and shaped NPs.

Ficus hispida L.f. (*F. hispida*; Moraceae), locally known as Kakdumur or dumoor, is prevalent in Bangladesh, forming a familiar sight in homesteads and village thickets. Native to southwest Asia, Thailand, the Mediterranean, India, Australia, Burma, and the Andaman Islands. All parts of this plant (such as root, stem, bark, leaves, fruits, and latex) have long served in treating ulcers, diabetes, jaundice, and more [45,46]. Recent studies have highlighted its diverse therapeutic potential, including cardioprotective effects, vaginal diseases, wound healing, anti-diarrheal, astringent, emetic, hepatic protective, antipyretic, antitussive, anti-inflammatory, vulnerary, depurative, hemostatic, anemia, and antiulcer agents, yet gaps persist in comprehending its full electrical activity [47,48]. Prior research emphasizes the plant's bioactive compounds like terpenoids, flavonoids, alkaloids, phenols, sterols, and glycosides and their role in multifaceted biological activities such as anti-proliferative effects on human breast cancer cells (T47D) [45,47,49]. Despite its traditional acclaim, scientific exploration of *F. hispida's* electrical activity (BECs) and antibacterial activities remains unexplored, necessitating further investigation to understanding the antimicrobial and electrical properties.

A ubiquitous gram-negative bacterium from the Enterobacteriaceae family, *Escherichia coli*, is found in both human and animal stomachs and in the environment [50,51]. It poses health risks as an opportunistic pathogen, causing various infections like diarrhea, enteritis, bacteremia, and urinary tract infections [52,53].

Staphylococcus epidermidis, typically part of the human skin's natural microbiota, is a non-aggressive gram-positive bacterium commonly present on skin and mucous membranes, including areas like the nose, armpits, and groin [54,55]. Normally considered part of the skin's natural flora, it's generally less harmful in healthy individuals. However, it can pose a threat when it enters the body through breaks in the skin or during surgical procedures, leading to infections, particularly in immune-compromised individuals or those with indwelling medical devices like catheters or prosthetic implants [56]. In such cases, *S. epidermidis* can cause infections such as bloodstream infections, surgical wound infections, and infections associated with medical devices, often due to its ability to form biofilms on surfaces, making eradication difficult [54].

Previous studies have utilized various plant extracts as electrolyte solutions, showcasing promising electrical performance. The organic acids present in plant extracts contribute H^+ ions to the electrolyte, while secondary salts like $CuSO_4.5H_2O$ accelerate cell reaction mechanisms [57]. In these cells, Zn releases electrons, which are accepted by Cu^{2+} and deposited on the cathode plate [58]. Zinc-based batteries have garnered attention for their potential in modern electronics due to their cost-effectiveness, safety, and high energy storage [59,60]. Aqueous Zn batteries, dating back to Volta's invention in 1799, offer high theoretical capacities and redox potential at a low cost, making metallic Zn an attractive electrode choice [61]. However, the corrosion rate of Zn anodes significantly impacts the sustainability of electrochemical cells, varying with the pH of the electrolyte solution [62].

The incorporation of Ag NPs as a catalyst in these electrochemical cells, alongside compounds like MnO_2, resulted in significant enhancements in electric voltage and current [63,64]. Bio-electrochemical cells, incorporating Ag NPs, enable electron transfer, offering a sustainable approach for electricity generation from organic or inorganic compounds. The enhanced performance of the fig extract-based BEC with integrated Ag NPs was highlighted by the study of four BEC configurations with various electrolytes. These configurations included higher short circuit current (I_{sc}), open circuit voltage (V_{oc}), maximum power (P_{max}), and decreased internal resistance (R_{in}). This research introduces a unique combination of two areas: investigating the antimicrobial potentials of FE mediated green-synthesized Ag NPs for biomedical applications and integrating a Zn/Cu electrode-based BEC cell. This groundbreaking BEC cell

employs fig extract as the organic electrolyte for electricity generation, afterward applying the Ag NPs as catalyst to enhance the electrical performance of BEC presenting a novel approach within this context for the first time.

2. Materials & methods

2.1. Collection of the fig and chemicals

The fig extract utilized in the experiments was prepared using freshly harvested figs sourced from Jhenaidah, Bangladesh. The silver nitrate ($AgNO_3$) employed in the experiments was obtained from Sigma-Aldrich Chemicals. Deionized (DI) water was used exclusively in all experimental procedures.

2.2. Preparation of the fig extract

Fresh figs underwent cleaning and chopping. Subsequently, 20 g of the figs were cooked at 60 °C for 1 h in 100 mL of DI water, with agitation provided by a heated magnetic stirrer. After cooling, the mixture underwent double filtration using Whatman No. 41 and No. 42 filter papers to eliminate impurities. After that, 4 °C was used to store the filtered FE.

2.3. Biosynthesis of FE_Ag NPs

Fig. 1 illustrates the synthesis of Ag NPs and the associated color changes observed during the synthesis process, initiated by combining 5 mL of freshly prepared aqueous FE with a 45 mL solution containing 0.005 M $AgNO_3$. Initially, the combined solution exhibited a brownish or dark brown color and was stored in a dark environment. As time elapsed, the color of the solution gradually transformed, indicating the formation of Ag NPs. The color change became more pronounced when the solution was exposed to FE, confirming of the successful bio-reduction of silver ions to Ag NPs.

2.4. Characterizations

Utilizing a Rigaku Smart Lab (Japan) equipped with a CuKα radiation source (λ = 1.54059 Å), scanning at 10° min^{-1}, and a tube current/voltage of 40 mA/40 kV, (XRD) investigation of biogenic Ag NPs was carried out. The crystalline phase was investigated at ambient temperature. UV–Vis spectrophotometry (U-2900) examined the spectrum from 200 to 1100 nm. FTIR spectrophotometry, utilizing a PerkinElmer FT-IR spectrophotometer (L1600300 Spectrum TWO LITA, UK), identified functional groups in fig extracts and Ag NPs. (FESEM) with a JSM-7610 F-equipped apparatus studied the silver nanoparticle morphology after coating with auto-fine platinum. Thermoscientific's Talos TEM investigated microstructures. A Clarus® 690 gas chromatograph and Clarus® SQ 8 C mass spectrophotometer (PerkinElmer, CA, USA) were used for the (GC-MS) study. The instruments were set up with a 1 μL sample, splitless mode, and helium carrier gas. The NIST database was employed for compound identification.

2.5. Bacteriological test of FE_Ag NPs

Mueller-Hinton agar was used to test the newly synthesized Ag NPs antibacterial activity against both gram-positive and gram-negative microorganisms using the disc diffusion technique. Bacterial strains (initial concentration: 1×10^8 CFU/mL) were provided by Jashore University of Science and Technology's Microbiology Department. For both concentrations, 10 μL of the extract solution was put onto each disk.

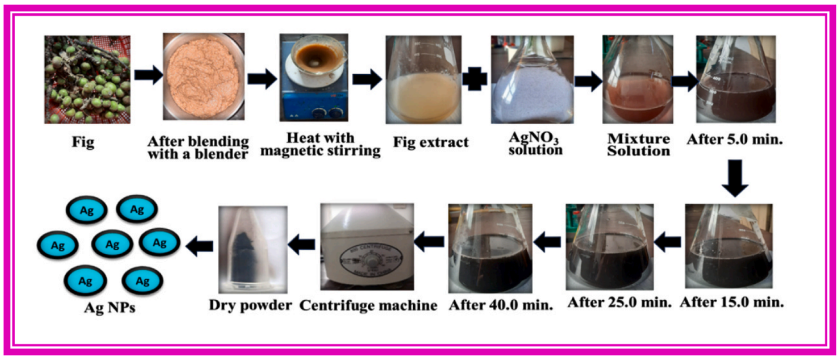

Fig. 1. Schematic representation of the color changes for producing silver nanoparticles using FE.

2.6. Designing FE_BEC structures

To assess the effects of Ag NPs on the power-generating system, four bio-electrochemical cells (Cells I, II, III, and IV) with Zn and Cu plates were employed, utilizing distinct electrolyte combinations detailed in Table 1 and illustrated in Fig. 2(a and b).

2.7. Connections between the anode and the cathode

Using Zn and Cu plates as electrodes and an electrolyte made of a combination of FE and green-synthesized Ag NPs catalyst, a BEC was built. The Zn plate served as the anode, releasing electrons, which were accepted by the Cu plate acting as the cathode. Cu atoms were deposited onto the Cu plate, and H_2 gas was formed at the cathode as a result of electron transfer processes involving electrons, H^+ ions, and Cu^{2+} ions in the electrolyte. Cu atoms were left behind on the Cu plate when the cell was opened, releasing H_2 gas [63].

3. Result and discussions

3.1. XRD analysis of FE_Ag NPs

XRD is frequently used to look at a substance's crystallinity by exposing samples to X-rays and analyzing patterns using Bragg's equation [65]. The diffraction peaks in Fig. 3 to the pertinent planes of (111), (200), (220), and (311) revealed the XRD pattern of FE-mediated silver nanoparticles at 38.34°, 44.54°, 64.68°, and 77.59° [66,67,68]. The XRD pattern matched JCPDS No. 65–2871, supporting Ag NPs FCC structure [69].

The average size of Ag NPs was approximately determined using the Debye-Scherrer formula in equation (1).

$$D = \frac{K\lambda}{\beta \, Cos \, \theta} \tag{1}$$

This equation relates the crystallite size (D) to various parameters such as Scherer's constant (K), radiation wavelength (λ), diffraction peak width (β), and Bragg angle (θ) [70,71]. According to this calculation, the Ag NPs were found to have an average crystallite size of 35.87 nm. However, this result diverged from the TEM-based estimation of 45.49 nm, as shown in Fig. 9. XRD sensitivity to coherent scattering domains might lead to variations in the actual particle size due to factors like lattice defects or amorphous surface layers induced by capping agents [72].

Bragg's law is a crucial tool for assessing properties like d-spacing, lattice constant (a), and unit cell volume (V) in nanoscale powders. Formula $2d \sin\theta = n\lambda$ or $d = \lambda/2 \sin\theta$ (with $n = 1$) determines the spacing between adjacent planes, where n is an integer representing the diffraction peak order, λ is the X-ray wavelength, and θ is the diffraction angle. The unit cell volume (V) is given by $V = a^3$. The approach involves using Bragg's law to find d-spacing (d_{hkl}) and then computing the lattice constant (a) with equation (2) [72]:

$$a = d_{hkl} \sqrt{h^2 + k^2 + l^2} \tag{2}$$

Where h, k, and l are Miller indices representing crystal plane orientation. Utilizing distinctive diffraction peaks for Ag NPs FCC structure, an average lattice constant of 0.4087 nm was determined (Table 2). This closely aligns with the JCPDS file's value (0.4086 nm) [73]. The lattice constant change indicated internal strain.

The Williamson-Hall (W–H) analysis was employed to refine outcomes by determining strain (ε) and distinguishing between size-induced and strain-induced peak broadening based on peak width and 2θ angle. Individual contributions to peak broadening were expressed as in equation (3)

$$\beta_{hkl} = \beta_s + \beta_D \tag{3}$$

where β_{hkl} is peak FWHM, β_s and β_D are size and strain widths [74]. Assuming uniform strain, β_{hkl} was given as

$$\beta_{hkl} = \frac{k\lambda}{\beta \cos\theta} + 4\varepsilon \tan\theta$$

Rearranging as equation (4)

Table 1
Electrolyte mixture.

Title of the Cell	Solution of electrolytes for bio-electrochemical cells
Cell-I	150 mL (FE)
Cell-II	150 mL (FE) + 50 mL (5 mg Ag NPs)
Cell-III	150 mL (FE) + $CuSO_4.5H_2O$ in 80 mL (1.2 M)
Cell-IV	150 mL (FE) + $CuSO_4.5H_2O$ in 80 mL (1.2 M) + 50 mL (5 mg Ag NPs)

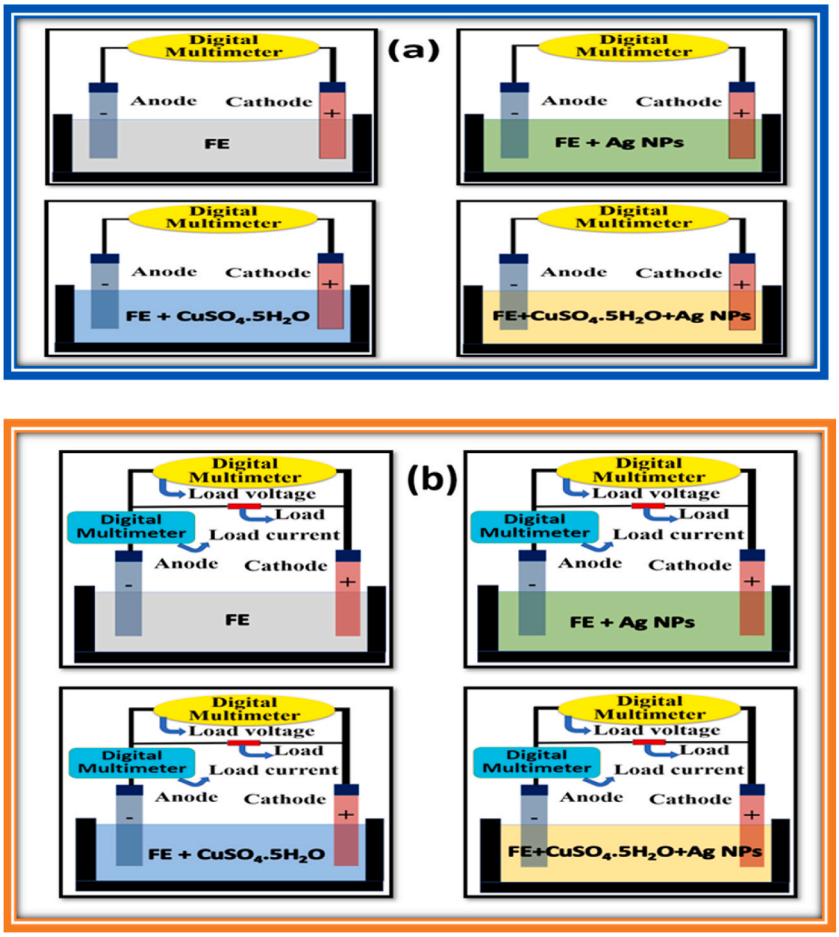

Fig. 2. Shows Zn/Cu-based FE_BEC setup (a) without and (b) with load circuit.

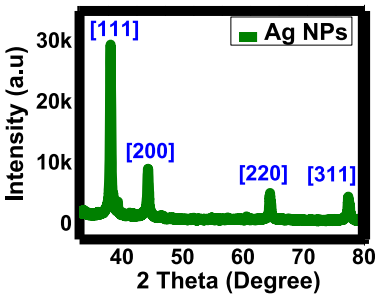

Fig. 3. XRD pattern for green synthesis Ag NPs.

Table 2
Geometric parameters of X-ray diffraction for Ag NPs.

θ position (°)	FWHM β (°)	Miller indices (*hkl*)	Crystallite size, D (nm)	d-spacing (nm)	Lattice parameter (a) nm
38.08477	0.2164	111	38.8353	0.23609	0.40892
44.29866	0.2712	200	31.6262	0.20431	0.40861
64.45046	0.2527	220	37.1612	0.14445	0.40857
77.41602	0.2839	311	35.8586	0.12318	0.40853
	Average values (nm)		35.8703	0.17701	0.40866

$$\beta_{hkl} \cos\theta = \frac{k\lambda}{D} + 4\varepsilon \sin\theta \tag{4}$$

By plotting (β_{hkl} cos θ) against (4 sin θ), strain ε was estimated the curve slope (Fig. 4). For the produced silver nanoparticles, particle size was determined as 34.66 nm, and strain as 5.97×10^{-5}. The crystal strain originated from imperfections and distortions the metallic nanoparticle crystal structure [72]. The details of the Williamson-Hall plotting data are shown in Table 3.

The application of stress to a crystal structure can create dislocations, influenced by factors like material morphology and crystalline size. The dislocation density is determined by Williamson-Smallman formula in equation (5) [75],

$$\delta = \frac{1}{D^2} \tag{5}$$

Dislocation density estimate for a 35.87 nm average crystal size (D). Dislocations warp the usual atomic arrangement and have a substantial impact on material characteristics. A value of 0.000777194 lines per nm^2 for Ag NPs highlights their strong crystallinity [76].

The width of material peaks in XRD data directly relates to average crystallite size, with crystalline materials displaying sharper peaks. In the XRD data of silver nanoparticles, peak broadening indicated a mean crystal size of 35.87 nm, determined through the Scherrer equation. The crystallinity index (I_{cry}) [77], given by equation (6)

$$I_{cry} = \frac{D_P\ (SEM, TEM)}{D_{cry}\ (XRD)}\ \left(I_{cry} \geq 1.00\right) \tag{6}$$

with an index of 1.24 (≥1.00), compares SEM or TEM particle size (D_p) to XRD-derived particle size (D_{cry}). An I_{cry} value near 1 suggests a monocrystalline structure, while higher values imply increased crystallinity in polycrystalline structures. For biosynthesized Ag NPs, I_{cry} surpassing 1.0 indicates strong crystallinity and a well-defined face-centered cubic (fcc) phase structure [73]. Table 4 presents the crystallinity index values derived from SEM or TEM particle sizes, all of which exceeded 1.0.

3.2. UV–visible spectral analysis of FE_Ag NPs

To confirm the presence of silver nanoparticles, UV–Visible spectroscopy was employed, a pivotal technique for structural characterization throughout the reduction process. UV–Vis spectroscopy monitors the synthesis and stability of nanoparticles. The spectra revealed a peak absorbance between 400 and 500 nm, indicative of the surface plasmon resonance (SPR) of the Ag NPs [78]. SPR absorbance intensity is influenced by particle size, shape, inter-particle distance, and the surrounding medium [78]. Fig. 5(a) depicts UV–visible spectra, showcasing Ag NPs synthesized through the green method (magenta line), fig extract (black line), DI water (blue line), $AgNO_3$ (red line). Fig. 5(b) represents the UV–visible spectra of Ag NPs alone and Fig. 5(c) shows the band gap analysis of Ag NPs. The confirmation of spherical or near-spherical Ag NPs is evidenced by the absorption peak at 418 nm. The addition of $AgNO_3$ to the fig extract, resulting in a shift towards a brownish color, suggests a reduction of silver ions (Ag^+) to elemental silver (Ag^0), facilitated by the fig extract's reducing agents. The band gap of Ag NPs was calculated at 5.23 eV by using Tauc plot. The Optical properties of silver nanoparticles correlate with diameter peaks from 412 to 420 nm in Fig. 5(b) imply sizes likely falling within the 40–50 nm range. These UV findings align with TEM and SEM analyses, confirming the synthesis of silver nanoparticles in the specified size range [79].

3.3. FTIR spectra analysis of FE_Ag NPs

FTIR analysis was conducted to identify biomolecules involved in the reduction of silver ions to silver nanoparticles using Fig extract. The analysis covered the wavenumber range of 400–4000 cm^{-1} [Fig. 6]. Peaks in the FTIR spectrum of the Fig extract at

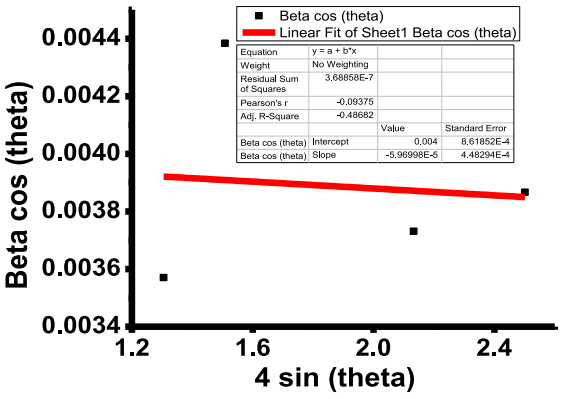

Fig. 4. Williamson–Hall analysis of Ag NPs.

Table 3
Presents the data for Williamson-Hall plotting, a technique to analyze the material's crystallite size and lattice strain.

2θ position (°)	FWHM β (°)	FWHM β (radians)	cos θ (radians)	β cos θ (radians)	4 sin θ	Particle size, D (nm)	Lattice strain (ϵ)	Dislocation density, δ (lines per nm^2)
38.08477	0.2164	0.00378	0.94528	0.00357	1.30507			
44.29866	0.2712	0.00473	0.92620	0.00438	1.50809	34.66	5.97×10^{-5}	0.000777194
64.45046	0.2527	0.00441	0.84596	0.00373	2.13300			
77.41602	0.2839	0.00496	0.78034	0.00387	2.50141			

Table 4
The crystallinity index based on SEM and TEM particle size.

Crystallite size, D_{cry} (nm)	Particle size, D_p (nm)		Crystallinity index, I_{cry} (unitless)		Particle type	
XRD	SEM	TEM	SEM	TEM	SEM	TEM
35.87	44.57	45.49	1.24	1.27	Mon crystalline	Mon crystalline

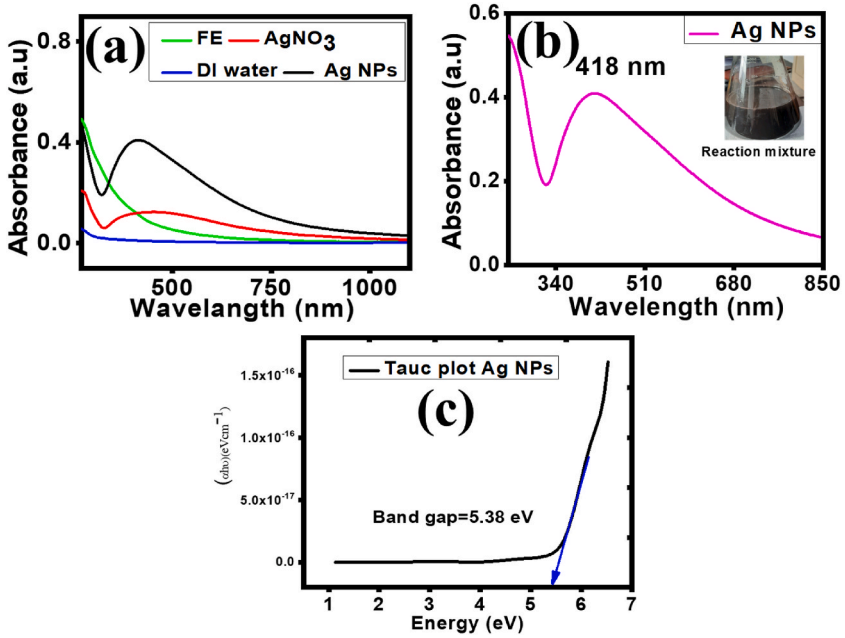

Fig. 5. UV–Vis spectra of (a) Ag NPs, fig extract, DI water, $AgNO_3$, (b) Ag NPs, and (c) band gap analysis of Ag NPs.

3435.22, 2359.96, 1652.70, 1558.68, 1456.96, 1048.12, and 667.73 cm^{-1} indicated the presence of functional groups crucial for the biosynthesis of metal nanoparticles. The 3435.22 cm^{-1} peak indicated alcohol or phenolic compounds, while the 1652.70 cm^{-1} peaks represented C═O and C═C bond stretching vibrations along with OH bending from bound water [80,81]. Notably, the Ag NPs exhibited narrower bands, indicating the reduction of silver ions. Peaks at 2359.96 cm^{-1} were associated with C ≡ C stretching vibration, 1456.96 cm^{-1} with C–H stretching of methyl groups and C–O–H bending, and 1048.12 cm^{-1} with C–*O*–H, –C═O, and C–H stretching bands of aromatic groups [20,42,63]. C═O stretching vibration occurred at 1558.68 cm^{-1} [41]. The Ag–O bond was seen at 667.73 cm^{-1} [70]. FTIR spectra indicated the involvement of carbonyl and hydroxyl groups in the reduction of Ag ions and their attachment to silver nanoparticles [70].

Comparing the FTIR spectra of fig extract-mediated Ag NPs, shifts in vibration frequencies are observed. Peaks shift from 3435.22 to 3447.62 cm^{-1}, 2359.96 to 2362.04 cm^{-1}, 1652.70 to 1653.18 cm^{-1}, 1456.96 to 1384.16 cm^{-1}, 1048.12 to 1039.44 cm^{-1}, and 667.73 to 665.73 cm^{-1}. Changes indicate silver ion reduction, capping, and stabilization of Ag NPs by biomolecules (alcohols, tannins, terpenes, terpenoids, and phenols) in fig extract [82,68]. Table 5 details functional groups in fig extract and Ag NPs.

3.4. Gas chromatography-mass spectrometry analysis

Fig. 7 depicts the chromatogram obtained from the GC-MS analysis of the fig extract. The chromatogram displays peaks corresponding to different chemical compounds present in the fig extract. The essential oils of plant extracts contain several important bio

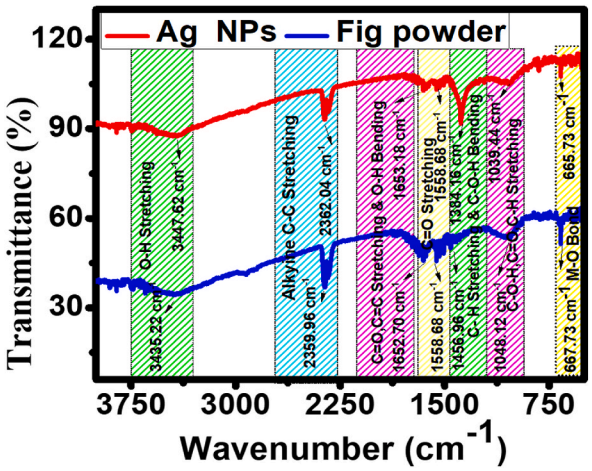

Fig. 6. Displays the FT-IR spectra of Ag NPs and fig powder.

Table 5
Gives a summary of the FTIR study of Ag NPs mediated by FE extract.

Functional Group	Wavenumber, n (cm^{-1})		
	Fig powder	**Ag NPs**	**Value of reference**
-OH hydroxyl group stretching vibration	3435.22	3447.62	3430 [80]
C ≡ C Vibrating stretching	2359.96	2362.04	2378 [63]
OH bending by bound water and stretching vibrations of C═O and C═C	1652.70	1653.18	1645 [81]
C═O stretching vibration of pyran typical of flavonoid C-rings,	1558.68	1558.68	1593 [41]
C–H stretching of methyl groups & C–O–H bending	1456.96	1384.16	1455 [42]
aromatic and C–*O*–H, –CO stretching vibration C–H vibrating stretched	1048.12	1039.44	1086 [20]
Ag O bond	667.73	665.73	682 [70]

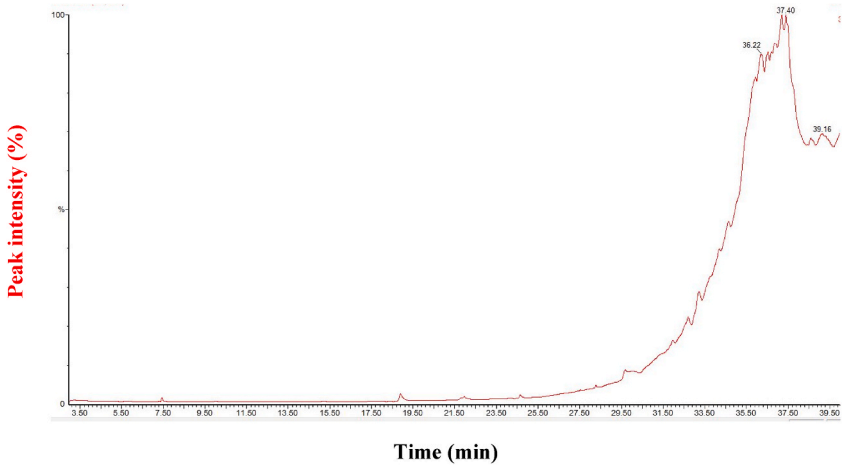

Fig. 7. Fig extract ethanol chromatogram by GCMS analysis.

compounds which may act as reducing as well as capping agent during the reaction mechanism of NPs and these bio compounds coated NPs shows excellent antimicrobial activities [83]. Each peak represents a specific compound detected by the GC-MS instrument, with the x-axis indicating the retention time (RT) in minutes and the y-axis representing the peak intensity or abundance of each compound. Eleven chemicals were found after GC-MS analysis of the fig extract. Table 6 offers a detailed breakdown of the bioactive components, including retention durations, peak regions, and molecular weights. Based on their relative abundance in the extract, the main ingredients—namely, 1,10-decanediol, 2tms derivative (0.69 %), phthalic anhydride (0.36 %), and 2,2,4-trimethyl-1,3-pentanediol diisobutyrate (0.18 %)—were identified.

Table 6
Analyzing fig extract components with GC-MS.

Serial No.	Retention time (RT)	Compounds	Molecular weight	Molecular Formula	Peak area (%)
1	7.44	Hentriacontane	436	$C_{31}H_{64}$	0.08
2	10.03	Ethanol, 2-[(phenylmethyl)amino]-	151	$C_9H_{13}ON$	0.04
3	18.44	Trifluoromethyltrimethylsilane	142	$C_4H_9F_3Si$	0.01
4	18.90	Phthalic anhydride	148	$C_8H_4O_3$	0.36
5	21.96	2,2,4-trimethyl-1,3-pentanediol diisobutyrate	286	$C_{16}H_{30}O_4$	0.18
6	24.21	3-chloropropanoic acid, 1-cyclopentylethyl ester	204	$C_{10}H_{17}O_2Cl$	0.02
7	24.64	Diethyl phthalate	222	$C_{12}H_{14}O_4$	0.08
8	24.99	Cyclodecasiloxane, eicosamethyl-	740	$C_{20}H_{60}O_{10}Si_{10}$	
9	27.54	Cyclooctasiloxane, hexadecamethyl-	592	$C_{16}H_{48}O_8Si_8$	0.01
10	28.29	Undecanoic acid, 10-methyl-, methyl ester	214	$C_{13}H_{26}O_2$	0.04
11	29.68	1,10-decanediol, 2tms derivative	318	$C_{16}H_{38}O_2Si_2$	0.69

3.5. FESEM analysis of FE_Ag NPs

FESEM images provide detailed insights into the size, shape, and distribution of synthesized Ag NPs, offering high-resolution, three-dimensional views of their surface morphology. They complement other techniques by revealing nanoparticle morphology, aggregation state, and interaction with sample components, enhancing overall structural characterization. The (FESEM) analysis (Fig. 8(a)) of Ag NPs synthesized using Fig extract revealed a predominantly spherical morphology with some irregular forms. FESEM analysis of irregular spherical shapes provides detailed morphology information, aiding in understanding nanoparticle formation mechanisms and optimizing synthesis conditions. ImageJ analysis (Fig. 8(b)) indicated a size range of 10 nm–90 nm, averaging 44.57 nm. Energy Dispersive X-ray Spectroscopy (EDX) displayed a 53.11 % silver content, confirming biosynthesis, while the prominent 3 keV peak in the EDX spectrum (Fig. 8(c and d)) verified elemental silver. A significant percentage of organic components (O, K, and C) indicated a strong coating of bio compound on the surface layer of green synthesized Ag NPs [84,85]. Hence, it is clearly understood that fig extract is acted not only for a reducing agent but also a strong capping agent during the synthesis method.

3.6. TEM analysis and zeta potential of FE_Ag NPs

TEM analysis provided an in-depth exploration of silver nanoparticles, revealing diverse shapes, with circles being predominant, as shown in Fig. 9(a and b). The fig extract played a dual role as a reducing and capping agent, preventing excessive aggregation for long-term stability. The crystalline structure of Ag NPs was shown by selected area electron diffraction (SAED) patterns (Fig. 9(c)). The size distribution histogram (Fig. 9(d)) highlighted predominantly spherical nanoparticles with diameters ranging from 20 to 70 nm. The average size of 45.49 nm is closely aligned with FESEM results, confirming the consistency of nanoparticle dimensions. Fig. 10 displays the zeta potential distribution of green synthesized Ag NPs. Zeta potential value was found −13.8 mV and this negative value reveal the stability as well as less agglomeration of Ag NPs [85].

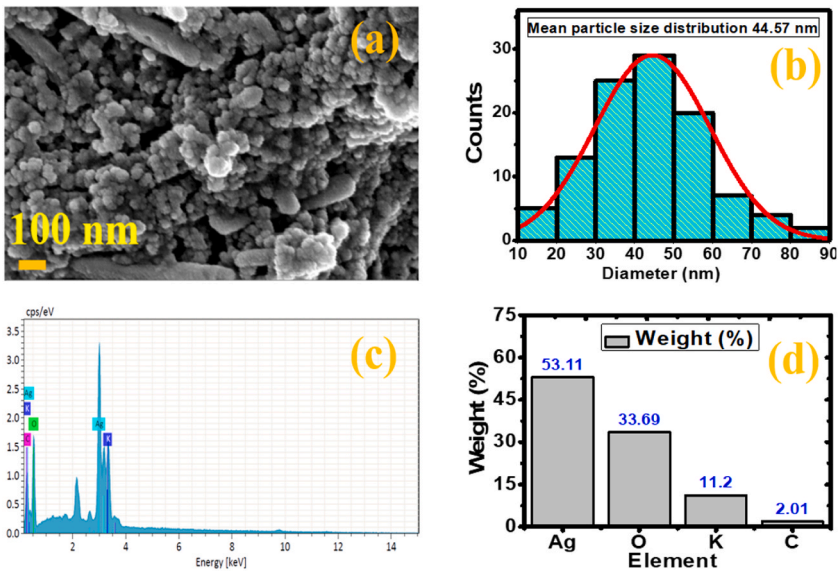

Fig. 8. Shows the Ag NPs (a) FESEM pictures, (b) mean particle size histogram, (c) EDX data, and (d) weight (%) of the constituents.

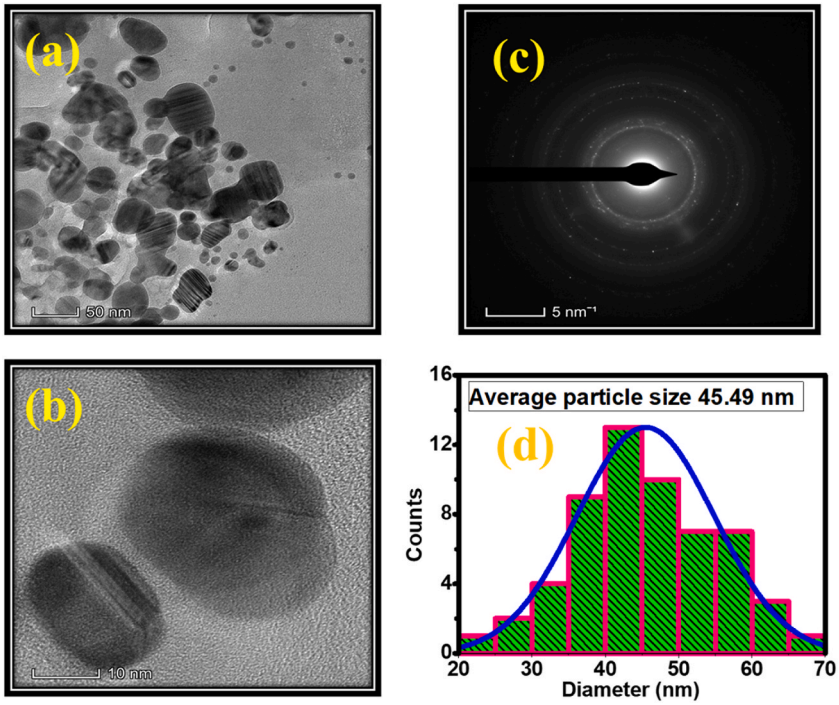

Fig. 9. Ag NPs TEM pictures at various sizes: (a) 50 nm, (b) 10 nm, (c) SAED pattern, and (d) particle size histogram.

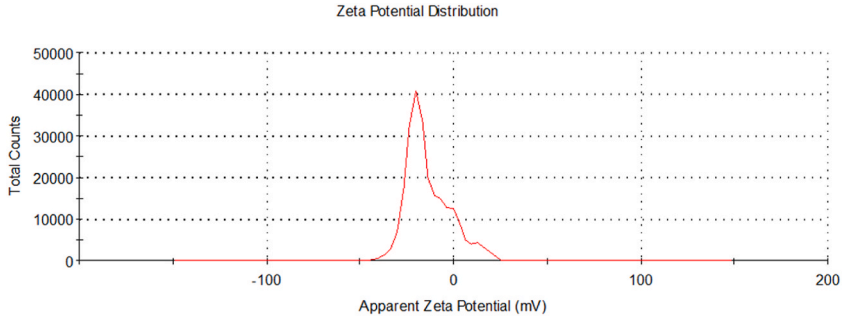

Fig. 10. Zeta potential distribution of FE mediated Ag NPs.

4. Antibacterial activity of FE_Ag NPs

Gram-positive and gram-negative bacterial strains were affected by FE_AgNPs, as demonstrated by the disc diffusion technique. Inhibition zones (mm) against *S. epidermidis* and *E. coli* at different AgNPs concentrations in comparison to azithromycin (the standard antibiotic, 6 mg/mL) are shown in Fig. 11(a–c). Inhibitory zones were measured at 17.30 ± 0.42 mm and 26.55 ± 0.50 mm for *E. coli* with 200 μg/disk and 400 μg/disk of FE_AgNPs, respectively. *S. epidermidis* exhibited zones of inhibition at 15.30 ± 0.28 mm and 21.50 ± 0.42 mm when treated with 200 μg/disk and 400 μg/disk of FE_AgNPs. Higher concentrations resulted in larger inhibition zones after 24 h at 37 °C. Table 7 presents the turbidimetry analysis of FE_AgNPs, confirming their potent antibacterial activity. Gram-negative bacteria displayed greater susceptibility to Ag NPs, likely due to differences in cell wall structure, with gram-positive bacteria having thicker peptidoglycan layers [80,86].

5. Electrical application of FE_Ag NPs

5.1. Power generation of BECs without load resistance

The study's findings were used to analyze how Ag NPs affected BECs ability to generate electricity. We created four cells using different electrolyte solutions, and we monitored their electrical abilities over time. The results, shown in Fig. 12(a–d), indicated that

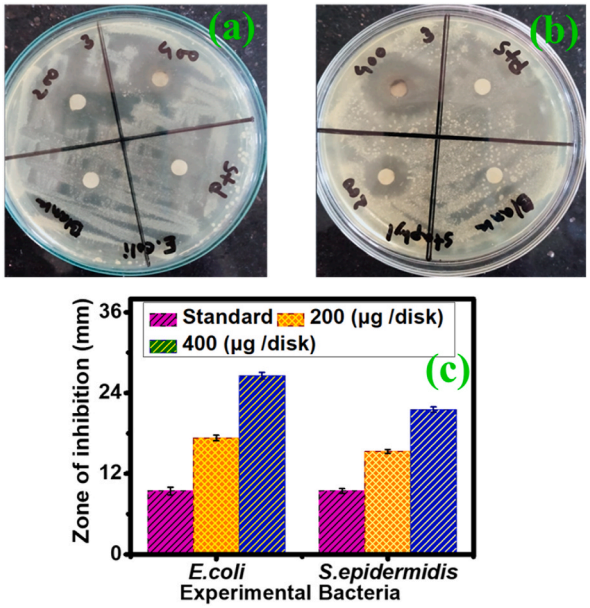

Fig. 11. Shows images (a, b) and bar graphs (c) comparing the antibacterial effects of silver nanoparticles and ethanol on specific bacteria.

Table 7
FE_AgNPs antibacterial effectiveness.

Organism	Common antibiotic (Azithromycin) (mm)	Limit of inhibition (mm) AgNPs (n = 2 samples for each concentration)	
		200 µg/disk	400 µg/disk
Escherichia coli	9.40 ± 0.57	17.30 ± 0.42	26.55 ± 0.50
Staphylococcus epidermidis	9.45 ± 0.35	15.30 ± 0.28	21.50 ± 0.42

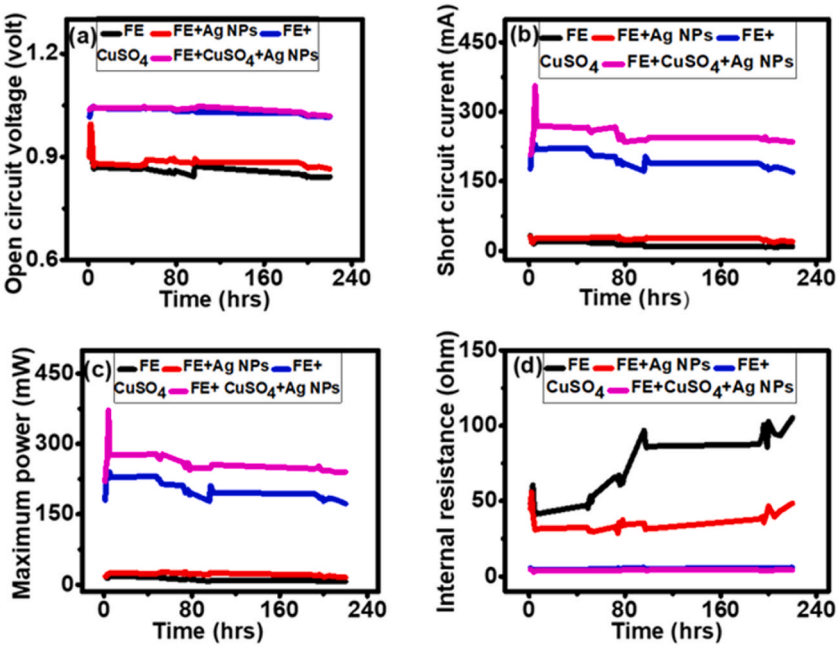

Fig. 12. Shows a cell's electrical activity for (a) V_{oc} b) I_{sc} (c) maximum power, and (d) internal resistance.

all cells were capable of generating electricity using fig extract electrolyte. Cell-IV, incorporating Ag NPs, displayed higher open-circuit voltage and short-circuit current compared to other cells, indicating lower internal resistance and the highest maximum power output (372.35 mW). In contrast, Cell-I exhibited the lowest maximum power output at 6.74 mW. The average electrical values of Cells I, II, III, and IV are contrasted in Table 8. Overall, the results indicate that adding Ag NPs can improve the ability of BECs to generate electricity.

5.2. Average voltage regulation and capacity

To analyze the electrical behavior of individual cells under a load of 6 Ω (6 Ω), a resistor was attached to each cell. The voltage and current across the load were then measured and documented over a specific period. Out of the four cells under study, Cell-IV showcased the most favorable electrical performance when compared to the others. Cell-IV employed a mixture of $CuSO_4.5H_2O$ and Ag NPs, along with an electrolyte solution derived from fig extract. As indicated by the information in Fig. 13(a–d), it was observed that the average voltage control of the BECs diminished when confronted with an external resistance of 6 Ω. Among the various cells investigated, Cell-IV had the largest capacity (0.61) and the lowest voltage regulation (0.28) among the cells.

5.3. Energy and voltage efficiency

Fig. 14(a and b) presents the comparison of the four cells under a 6-Ω load resistance. Average voltage efficiency and energy efficiency were calculated, showing enhanced performance in bio-electrochemical cells. Notably, Cell-IV surpassed others, achieving 78.59 % voltage efficiency and 68.69 % energy efficiency, demonstrating critical improvements.

Therefore, this work looked at the impact of Ag NPs on the cell and performed a basic analysis of fig extract-based BECs. The modified electrolyte consisting of FE, $CuSO_4$, and Ag NPs significantly improved the electrical performances of the bio-electrochemical cell. The increased electrical activity of Cell-IV revealed the amazing ability of Ag NPs to provide inexpensive power, indicating the possibility of creating a bio-electrochemical module with Ag NP integration.

6. Conclusion and recommendations

This study showcases advancements in characterizing and utilizing fig extract-mediated Ag NPs, revealing heightened antibacterial efficacy and superior electrical performance of FE in bio-electrochemical cells. The formation of FCC Ag NPs using fig fruit extract as a reducing agent was confirmed by UV–vis spectra, followed by the XRD date of Ag NPs. The active functional groups of organic compounds were manifested in the FTIR spectra of FE and Ag NPs. The high-resolution FESEM and TEM images with EDX data revealed mostly the spherical formation of biogenic Ag NPs. However, the antimicrobial properties of FE-mediated Ag NPs were probed against *S. epidermidis* and *E. coli* bacteria by the disk diffusion method. A higher concentration of Ag NPs exhibited a higher inhibition zone against both pathogens. Ag NPs acted more efficiently against gram-negative bacteria *E. coli* than gram-positive bacteria *S. epidermidis* because gram-negative bacteria have a comparatively thinner cell wall. Fig fruit extract was used as a bio-electrolyte solution in an electrochemical cell to generate electricity. The electrical power was determined by recording the open-circuit voltage and short-circuit current of the fig extract electrolyte-based electrochemical cell. The electrical performance of cells has been enhanced by incorporating Ag NPs. Hence, this report successfully demonstrated the power generation activities of FE through electrochemical cells, and green synthesized Ag NPs played an active role as catalysts to integrate the electrical performance of cells. Though the current study showed electricity generation by fig extract, the commercial uses of such a cell need further investigation on a large scale. The versatile uses of fig extract have been explored by this study, and the findings may open a new era for nano-biotechnology.

Data availability

All data are reported in this manuscript and date will be available upon the request.

CRediT authorship contribution statement

Md Ohiduzzaman: Writing – original draft, Methodology, Investigation, Funding acquisition, Formal analysis, Data curation, Conceptualization. **M.N.I. Khan:** Writing – review & editing, Supervision. **K.A. Khan:** Writing – review & editing, Supervision, Funding acquisition, Conceptualization. **Bithi Paul:** Writing – review & editing, Formal analysis, Data curation, Conceptualization. **Md Nazmul Hasan Zilani:** Investigation, Formal analysis. **Md Nazmul Hasan:** Investigation, Formal analysis.

Table 8
Presents the standard electrical properties of BEC.

Name of the cell	Average power (watt)	Average internal resistance (ohm)	Average voltage regulation for 6 Ω
Cell- I	0.01164	70.44162	15.03679
Cell- II	0.02215	36.511827	9.86378
Cell- III	0.2032	5.285305	0.93957
Cell- IV	0.2594	4.173768	0.27708

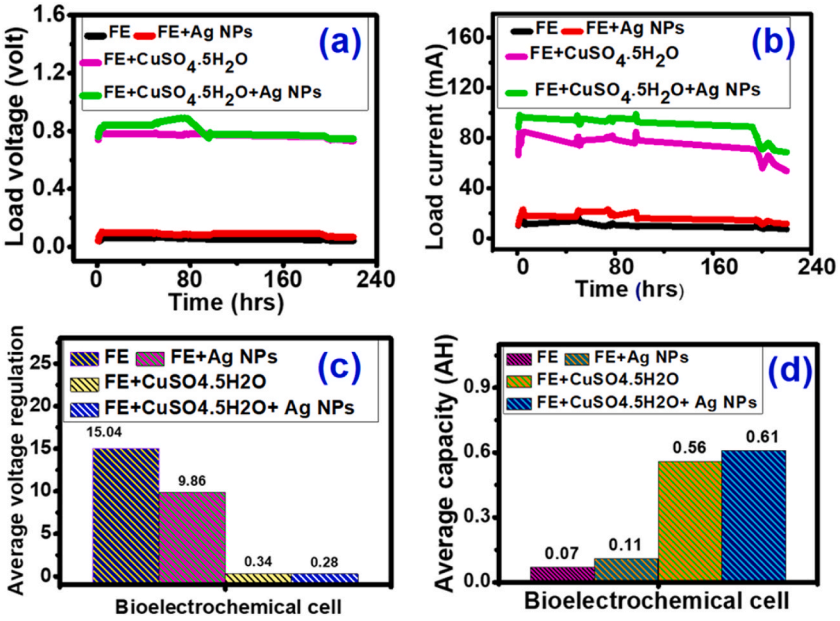

Fig. 13. Illustrates the electrical behavior within the cells, depicting (a) load voltage, (b) load current, (c) voltage regulation, and (d) capacity for a load resistance of 6 Ω.

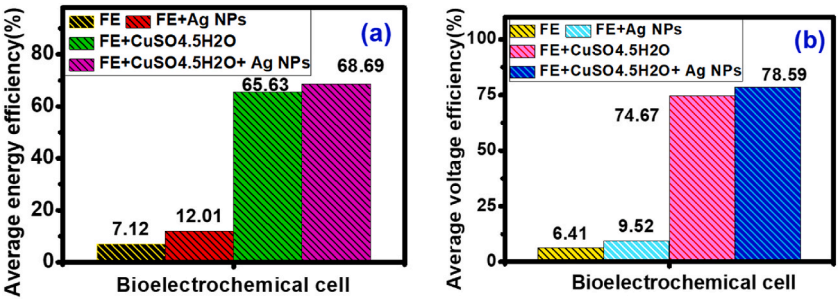

Fig. 14. Shows the average (a) energy and (b) voltage efficiency of 6 Ω load resistances.

Declaration of competing interest

The authors declare the following financial interests/personal relationships which may be considered as potential competing interests:

Md. Ohiduzzaman reports financial support was provided by Government of the People's Republic of Bangladesh Ministry of Science and Technology. If there are other authors, they declare that they have no known competing financial interests or personal relationships that could have appeared to influence the work reported in this paper.

Acknowledgments

This work is supported by the NST (National Science and Technology) Fellowship, Ministry of Science and Technology, Government of Bangladesh (GoB) (Award Id: 120005100-3821117). The authors would like to acknowledge the Laboratory of Pharmaceutical Biotechnology and Bioinformatics, Department of Genetic Engineering and Biotechnology, Jashore University of Science and Technology, Jashore-7408, and Materials Science Division, Atomic Energy Centre, Dhaka, Bangladesh to provide the required facilities during this research.

References

[1] N. Joudeh, D. Linke, Nanoparticle classification, physicochemical properties, characterization, and applications: a comprehensive review for biologists, J. Nanobiotechnol. 20 (2022) 262, https://doi.org/10.1186/s12951-022-01477-8.

[2] A. GulFozia, A. Shaheen, I. Ahmad, B. Khattak, M. Ahmad, R. Ullah, A. Bari, S.S. Ali, A. Alobaid, M.M. Asmari, H.M. Mahmood, Green synthesis, characterization, enzyme inhibition, antimicrobial potential, and cytotoxic activity of plant mediated silver nanoparticle using Ricinus communis leaf and root extracts, Biomolecules 11 (2021) 206, https://doi.org/10.3390/biom11020206.

[3] A.G. Sivakov, R.P. Yavetskiy, N.A. Matveevskaya, T.G. Beynik, A.V. Tolmachev, S.I. Bondarenko, A.S. Pokhila, A.V. Krevsun, V.P. Koverya, A.S. Garbuz, Study of electrical conductivity of the coatings of bimetallic Au-Ag nanoparticles, Phys. E Low-dimens. Syst. Nanostruct. 120 (2020) 114091, https://doi.org/10.1016/j.physe.2020.114091.

[4] C.Y. Rahimzadeh, A.A. Barzinjy, A.S. Mohammed, S.M. Hamad, Green synthesis of SiO2 nanoparticles from Rhus coriaria L. extract: comparison with chemically synthesized SiO2 nanoparticles, PLoS One 17 (8) (2022 Aug 5) e0268184, https://doi.org/10.1371/journal.pone.0268184.

[5] X. You, G. Zhang, Y. Chen, D. Liu, D. Ma, J. Zhou, Y. Liu, H. Liu, Y. Qi, C. Liang, P. Ding, X. Zhu, C. Zhang, A. Wang, A novel electrochemical immunosensor for the sensitive detection of tiamulin based on staphylococcal protein A and silver nanoparticle-graphene oxide nanocomposites, Bioelectrochemistry 141 (2021) 107877, https://doi.org/10.1016/j.bioelechem.2021.107877.

[6] S. Gajbhiye, S. Sakharwade, Silver nanoparticles in cosmetics, JCDSA 06 (2016) 48–53, https://doi.org/10.4236/jcdsa.2016.61007.

[7] P. Banerjee, M. Satapathy, A. Mukhopahayay, P. Das, Leaf extract mediated green synthesis of silver nanoparticles from widely available Indian plants: synthesis, characterization, antimicrobial property and toxicity analysis, Bioresour. Bioprocess. 1 (2014) 3, https://doi.org/10.1186/s40643-014-0003-y.

[8] N.K. Sharma, J. Vishwakarma, S. Rai, T.S. Alomar, N. AlMasoud, A. Bhattarai, Green route synthesis and characterization techniques of silver nanoparticles and their biological adeptness, ACS Omega 7 (2022) 27004–27020, https://doi.org/10.1021/acsomega.2c01400.

[9] A.A. Barzinjy, V.N. adamen, Investigating physical properties and formation mechanism of biosynthesized zinc oxide nanoparticles using dill (Anethum graveolens) leaf extract, Nanosci. Nanotechnol. - Asia 12 (6) (2022 Dec 1) 27–38, https://doi.org/10.2174/2210681213666221114094914.

[10] Z. Saeed, M. Pervaiz, A. Ejaz, S. Hussain, S. Shaheen, B. Shehzad, U. Younas, Garlic and ginger extracts mediated green synthesis of silver and gold nanoparticles: a review on recent advancements and prospective applications, Biocatal. Agric. Biotechnol. 53 (2023) 102868, https://doi.org/10.1016/j.bcab.2023.102868.

[11] H.H. Azeez, A.A. Barzinjya, S.M. Hamad, Structure, synthesis and applications of ZnO nanoparticles:A review, Jordan Journal of Physics 13 (2) (2020) 123–135. https://www.researchgate.net/publication/342347708.

[12] S.M. Mustafa, A.A. Barzinjy, A.H. Hamad, S.M. Hamad, Betaine-based deep eutectic solvents mediated synthesis of zinc oxide nanoparticles at low temperature, Ceram. Int. 48 (19) (2022 Oct 1) 28951–28960, https://doi.org/10.1016/j.ceramint.2022.04.131.

[13] P. Boomi, R.M. Ganesan, G. Poorani, H. Gurumallesh Prabu, S. Ravikumar, J. Jeyakanthan, Biological synergy of greener gold nanoparticles by using Coleus aromaticus leaf extract, Mater. Sci. Eng. C 99 (2019) 202–210, https://doi.org/10.1016/j.msec.2019.01.105.

[14] A.A. Barzinjy, B.S. Haji, H. Fouad, Green synthesis of silver nanoparticles using Citrullus colocynthis fruit extract and the eutectic-based ionic liquid: thin film application, J. Nanoelectron. Optoelectron. 17 (10) (2022 Oct 1) 1328–1342, https://doi.org/10.1166/jno.2022.3324.

[15] S.A. Khan, S. Shahid, C.-S. Lee, Green synthesis of gold and silver nanoparticles using leaf extract of clerodendrum inerme; characterization, antimicrobial, and antioxidant activities, Biomolecules 10 (2020) 835, https://doi.org/10.3390/biom10060835.

[16] M.S. Samuel, M. Ravikumar, A. John J, E. Selvarajan, H. Patel, P.S. Chander, J. Soundarya, S. Vuppala, R. Balaji, N. Chandrasekar, A review on green synthesis of nanoparticles and their diverse biomedical and environmental applications, Catalysts 12 (2022) 459, https://doi.org/10.3390/catal12050459.

[17] Y.T. Gebreslassie, H.G. Gebretnsae, Green and cost-effective synthesis of tin oxide nanoparticles: a review on the synthesis methodologies, mechanism of formation, and their potential applications, Nanoscale Res. Lett. 16 (2021) 97, https://doi.org/10.1186/s11671-021-03555-6.

[18] N.S. Alsaiari, F.M. Alzahrani, A. Amari, H. Osman, H.N. Harharah, N. Elboughdiri, M.A. Tahoon, Plant and microbial approaches as green methods for the synthesis of nanomaterials: synthesis, applications, and future perspectives, Molecules 28 (2023) 463, https://doi.org/10.3390/molecules28010463.

[19] N.S. Piro, S.M. Hamad, A.S. Mohammed, A.A. Barzinjy, Green synthesis magnetite (Fe_3O_4) nanoparticles from Rhus coriaria extract: a characteristic comparison with a conventional chemical method, IEEE Trans. NanoBioscience 22 (2) (2022 Jun 30) 308–317, https://doi.org/10.1109/TNB.2022.3187344.

[20] S. Mortazavi-Derazkola, M.A. Ebrahimzadeh, O. Amiri, H.R. Goli, A. Rafiei, M. Kardan, M. Salavati-Niasari, Facile green synthesis and characterization of Crataegus microphylla extract-capped silver nanoparticles (CME@Ag-NPs) and its potential antibacterial and anticancer activities against AGS and MCF-7 human cancer cells, J. Alloys Compd. 820 (2020) 153186, https://doi.org/10.1016/j.jallcom.2019.153186.

[21] A.A. Barzinjy, Biofabrication of Ag nanoparticles using bacteria, plant fungi and algae and their applications in clinical gadgets, Eurasian Journal of Science & Engineering 8 (2) (2022), https://doi.org/10.23918/eajse.v8i2p101.

[22] R.F. Talabani, S.M. Hamad, A.A. Barzinjy, U. Demir, Biosynthesis of silver nanoparticles and their applications in harvesting sunlight for solar thermal generation, Nanomaterials 11 (9) (2021 Sep 17) 2421, https://doi.org/10.3390/nano11092421.

[23] R.F. Talabani, S.M. Hamad, A.A. Barzinjy, U. Demir, Biosynthesis of silver nanoparticles and their applications in harvesting sunlight for solar thermal generation, Nanomaterials 11 (9) (2021 Sep 17) 2421, https://doi.org/10.3390/nano11092421.

[24] S.B. Haji, A.A. Barzinjy, The status of green synthesis of silver nanoparticles using plant extracts during last fifteen years, Jordan Journal of Physics 15 (5) (2022) 429–444, https://doi.org/10.47011/15.5.1.

[25] V.M. Faris, A.A. Barzinjy, S.M. Hamad, Biosynthesis of silver nanoparticles at various pH values and their applications in capturing irradiation, Solar Energy, Recent Patents on Nanotechnology 18 (1) (2024 Feb 1) 54–71, https://doi.org/10.2174/1872210516666220826143110.

[26] B.S. Haji, A.A. Barzinjy, Citrullus colocynthis fruit extract mediated green synthesis of silver nanoparticles: the impact of pH, temperature, and silver nitrate concentration, e-J. Surf. Sci. Nanotechnol. 21 (1) (2022 Dec 3) 61–71, https://doi.org/10.1380/ejssnt.2023-010.

[27] A.A. Barzinjy, The Applications of Green Synthesized Silver Nanoparticles: Review 8 (2) (2022), https://doi.org/10.23918/eajse.v8i2p16. https://eajse.tiu.edu.iq/index.php/volume-8-issue-2-article-3/.

[28] A. Palma, M.J. Díaz, M. Ruiz-Montoya, E. Morales, I. Giráldez, Ultrasound extraction optimization for bioactive molecules from Eucalyptus globulus leaves through antioxidant activity, Ultrason. Sonochem. 76 (2021) 105654, https://doi.org/10.1016/j.ultsonch.2021.105654.

[29] S.Y. Chew, S.Y. Teoh, Y.Y. Sim, K.L. Nyam, Optimization of ultrasonic extraction condition for maximal antioxidant, antimicrobial, and antityrosinase activity from Hibiscus cannabinus L. leaves by using the single factor experiment, Journal of Applied Research on Medicinal and Aromatic Plants 25 (2021) 100321, https://doi.org/10.1016/j.jarmap.2021.100321.

[30] C. Singh, S.K. Anand, R. Upadhyay, N. Pandey, P. Kumar, D. Singh, P. Tiwari, R. Saini, K.N. Tiwari, S.K. Mishra, R. Tilak, Green synthesis of silver nanoparticles by root extract of Premna integrifolia L. and evaluation of its cytotoxic and antibacterial activity, Mater. Chem. Phys. 297 (2023) 127413, https://doi.org/10.1016/j.matchemphys.2023.127413.

[31] S.B. Zimare, G.D. Mankar, R.B. Barmukh, Optimization of ultrasound-assisted extraction of total phenolics and flavonoids from the leaves of Lobelia nicotianifolia and their radical scavenging potential, Current Research in Green and Sustainable Chemistry 4 (2021) 100109, https://doi.org/10.1016/j.crgsc.2021.100109.

[32] E.O. Oke, O. Adeyi, B.I. Okolo, J.A. Adeyi, J. Ayanyemi, K.A. Osoh, T.S. Adegoke, Phenolic compound extraction from Nigerian Azadirachta Indica leaves: response surface and neuro-fuzzy modelling performance evaluation with Cuckoo Search multi-objective optimization, Results in Engineering 8 (2020) 100160, https://doi.org/10.1016/j.rineng.2020.100160.

[33] V. Sablania, S.J.D. Bosco, Optimization of spray drying parameters for Murraya koenigii (Linn) leaves extract using response surface methodology, Powder Technol. 335 (2018) 35–41, https://doi.org/10.1016/j.powtec.2018.05.009.

[34] A. Nekkaa, A. Benaissa, A.E.D. Lalaouna, F. Mutelet, L. Canabady-Rochelle, Optimization of the extraction process of bioactive compounds from Rhamnus alaternus leaves using Box-Behnken experimental design, Journal of Applied Research on Medicinal and Aromatic Plants 25 (2021) 100345, https://doi.org/10.1016/j.jarmap.2021.100345.

[35] K. Ameer, S.-W. Bae, Y. Jo, H.-G. Lee, A. Ameer, J.-H. Kwon, Optimization of microwave-assisted extraction of total extract, stevioside and rebaudioside-A from Stevia rebaudiana (Bertoni) leaves, using response surface methodology (RSM) and artificial neural network (ANN) modelling, Food Chem. 229 (2017) 198–207, https://doi.org/10.1016/j.foodchem.2017.01.121.

[36] P.V. de Almeida Pontes, I. Ayumi Shiwaku, G.J. Maximo, E.A. Caldas Batista, Choline chloride-based deep eutectic solvents as potential solvent for extraction of phenolic compounds from olive leaves: extraction optimization and solvent characterization, Food Chem. 352 (2021) 129346, https://doi.org/10.1016/j.foodchem.2021.129346.
[37] M.S. Hasnain, MdN. Javed, MdS. Alam, P. Rishishwar, S. Rishishwar, S. Ali, A.K. Nayak, S. Beg, Purple heart plant leaves extract-mediated silver nanoparticle synthesis: optimization by Box-Behnken design, Mater. Sci. Eng. C 99 (2019) 1105–1114, https://doi.org/10.1016/j.msec.2019.02.061.
[38] S. Raj, H. Singh, R. Trivedi, V. Soni, Biogenic synthesis of AgNPs employing Terminalia arjuna leaf extract and its efficacy towards catalytic degradation of organic dyes, Sci. Rep. 10 (2020) 9616, https://doi.org/10.1038/s41598-020-66851-8.
[39] N.N. Fard, H. Noorbazargan, A. Mirzaie, M. Hedayati Ch, Z. Moghimiyan, A. Rahimi, Biogenic synthesis of AgNPs using *Artemisia oliveriana* extract and their biological activities for an effective treatment of lung cancer, Artificial Cells, Nanomedicine, and Biotechnology 46 (2018) 1047–1058, https://doi.org/10.1080/21691401.2018.1528983.
[40] F.A. Lubis, N.A.N.N. Malek, N.S. Sani, K. Jemon, Biogenic synthesis of silver nanoparticles using Persicaria odorata leaf extract: antibacterial, cytocompatibility, and in vitro wound healing evaluation, Particuology 70 (2022) 10–19, https://doi.org/10.1016/j.partic.2022.01.001.
[41] W.M. Alamier, M. D Y Oteef, A.M. Bakry, N. Hasan, K.S. Ismail, F.S. Awad, Green synthesis of silver nanoparticles using *Acacia ehrenbergiana* plant Cortex extract for efficient removal of rhodamine B cationic dye from wastewater and the evaluation of antimicrobial activity, ACS Omega 8 (2023) 18901–18914, https://doi.org/10.1021/acsomega.3c01292.
[42] P. Saha, Md Mahiuddin, A.B.M.N. Islam, B. Ochiai, Biogenic synthesis and catalytic efficacy of silver nanoparticles based on peel extracts of *Citrus macroptera* fruit, ACS Omega 6 (2021) 18260–18268, https://doi.org/10.1021/acsomega.1c02149.
[43] A. Wirwis, Z. Sadowski, Green synthesis of silver nanoparticles: optimizing green tea leaf extraction for enhanced physicochemical properties, ACS Omega 8 (2023) 30532–30549, https://doi.org/10.1021/acsomega.3c03775.
[44] M. Soltani Nejad, N. Samandari Najafabadi, S. Aghighi, M. Zargar, Phytosynthesis of silver nanoparticles by Paulownia fortunei fruit exudates and its application against Fusarium sp. causing dry rot postharvest diseases of banana, Biocatal. Agric. Biotechnol. 54 (2023) 102949, https://doi.org/10.1016/j.bcab.2023.102949.
[45] J. Zhang, W. Zhu, J. Xu, W. Kitdamrongtham, A. Manosroi, J. Manosroi, H. Tokuda, M. Abe, T. Akihisa, F. Feng, Potential cancer chemopreventive and anticancer constituents from the fruits of Ficus hispida L.f. (Moraceae), J. Ethnopharmacol. 214 (2018) 37–46, https://doi.org/10.1016/j.jep.2017.11.016.
[46] X.-Y. Jia, Y.-M. Wu, J.-Y. Li, C. Lei, A.-J. Hou, Alkaloid constituents of Ficus hispida and their antiinflammatory activity, Nat. Prod. Bioprospect. 10 (2020) 45–49, https://doi.org/10.1007/s13659-020-00233-5.
[47] J. Cheng, B. Zhang, W. Zhu, C. Zhang, Y. Qin, M. Abe, T. Akihisa, W. Liu, F. Feng, J. Zhang, Traditional uses, phytochemistry, and pharmacology of Ficus hispida L.f.: a review, J. Ethnopharmacol. 248 (2020) 112204, https://doi.org/10.1016/j.jep.2019.112204.
[48] P. Deepa, K. Sowndhararajan, S. Kim, S.J. Park, A role of Ficus species in the management of diabetes mellitus: a review, J. Ethnopharmacol. 215 (2018) 210–232, https://doi.org/10.1016/j.jep.2017.12.045.
[49] K. Kanagamani, P. Muthukrishnan, M. Ilayaraja, K. Shankar, A. Kathiresan, Synthesis, characterisation and DFT studies of stigmasterol mediated silver nanoparticles and their anticancer activity, J. Inorg. Organomet. Polym. 28 (2018) 702–710, https://doi.org/10.1007/s10904-017-0721-7.
[50] A.M. Awad, N.A. El-Shall, D.S. Khalil, M.E.A. El-Hack, A.A. Swelum, A.H. Mahmoud, H. Ebaid, A. Komany, R.H. Sammour, M.E. Sedeik, Incidence, pathotyping, and antibiotic susceptibility of avian pathogenic Escherichia coli among diseased broiler chicks, Pathogens 9 (2020) 114, https://doi.org/10.3390/pathogens9020114.
[51] C. Xu, L. Kong, Y. Liao, Y. Tian, Q. Wu, H. Liu, X. Wang, Mini-review: antibiotic-resistant Escherichia coli from farm animal-associated sources, Antibiotics 11 (2022) 1535, https://doi.org/10.3390/antibiotics11111535.
[52] J.-W. Chen, H.H. Huang, S.-M. Chang, J. Scaria, Y.-L. Chiu, C.-M. Chen, W.-C. Ko, J.-L. Wang, Antibiotic-Resistant Escherichia coli and sequence type 131 in fecal colonization in dogs in taiwan, Microorganisms 8 (2020) 1439, https://doi.org/10.3390/microorganisms8091439.
[53] A.S. Singh, B.B. Nayak, S.H. Kumar, High prevalence of multiple antibiotic-resistant, extended-spectrum β-lactamase (ESBL)-Producing Escherichia coli in fresh seafood sold in retail markets of Mumbai, India, Veterinary Sciences 7 (2020) 46, https://doi.org/10.3390/vetsci7020046.
[54] J.Y.H. Lee, I.R. Monk, A. Gonçalves da Silva, T. Seemann, K.Y.L. Chua, A. Kearns, R. Hill, N. Woodford, M.D. Bartels, B. Strommenger, F. Laurent, M. Dodémont, A. Deplano, R. Patel, A.R. Larsen, T.M. Korman, T.P. Stinear, B.P. Howden, Global spread of three multidrug-resistant lineages of Staphylococcus epidermidis, Nat Microbiol 3 (2018) 1175–1185, https://doi.org/10.1038/s41564-018-0230-7.
[55] K. Perez, R. Patel, Survival of Staphylococcus epidermidis in fibroblasts and osteoblasts, Infect. Immun. 86 (2018) e00237, https://doi.org/10.1128/IAI.00237-18. -18.
[56] T.J. Foster, Surface proteins of Staphylococcus epidermidis, Front. Microbiol. 11 (2020) 1829, https://doi.org/10.3389/fmicb.2020.01829.
[57] M. Hasan, K.A. Khan, Dynamic model of Bryophyllum pinnatum leaf fueled BPL cell: a possible alternate source of electricity at the off-grid region in Bangladesh, Microsyst. Technol. 25 (2019) 2481–2492, https://doi.org/10.1007/s00542-018-4149-y.
[58] K.A. Khan, M.H. Ali, M.A. Mamun, M.M. Haque, A.K.M.A. Ullah, M.N.I. Khan, L. Hassan, A.K.M. Obaydullah, M.A. Wadud, Bioelectrical characterization and production of nanoparticles (NPs) using PKL extract for electricity generation, Microsyst. Technol. 28 (2022) 823–832, https://doi.org/10.1007/s00542-020-04774-0.
[59] X. Yu, F. Hu, Z.-Q. Guo, L. Liu, G.-H. Song, K. Zhu, High-performance Cu0.95V2O5 nanoflowers as cathode materials for aqueous zinc-ion batteries, Rare Met. 41 (2022) 29–36, https://doi.org/10.1007/s12598-021-01771-8.
[60] J. Hao, X. Li, X. Zeng, D. Li, J. Mao, Z. Guo, Deeply understanding the Zn anode behaviour and corresponding improvement strategies in different aqueous Zn-based batteries, Energy Environ. Sci. 13 (2020) 3917–3949, https://doi.org/10.1039/D0EE02162H.
[61] B. Scrosati, History of lithium batteries, J. Solid State Electrochem. 15 (2011) 1623–1630, https://doi.org/10.1007/s10008-011-1386-8.
[62] Z. Cai, J. Wang, Y. Sun, Anode corrosion in aqueous Zn metal batteries, eScience 3 (2023) 100093, https://doi.org/10.1016/j.esci.2023.100093.65.
[63] M.A. Hossain, B. Paul, K.A. Khan, M. Paul, M.A. Mamun, M.E. Quayum, Green synthesis and characterization of silver nanoparticles by using Bryophyllum pinnatum and the evaluation of its power generation activities on bio-electrochemical cell, Mater. Chem. Phys. 282 (2022) 125943, https://doi.org/10.1016/j.matchemphys.2022.125943.
[64] K.A. Khan, B. Paul, M.A.K. Siddique, M. Paul, S.M. Zian Reza, Electrical activities of ginger extract-mediated silver nanoparticles in bio-electrochemical cell, in: T.R. Lenka, S.K. Saha, L. Fu (Eds.), Micro and Nanoelectronics Devices, Circuits and Systems, Springer Nature Singapore, Singapore, 2024, pp. 483–491, https://doi.org/10.1007/978-981-99-4495-8_38.
[65] K.C. Hembram, R. Kumar, L. Kandha, P.K. Parhi, C.N. Kundu, B.K. Bindhani, Therapeutic prospective of plant-induced silver nanoparticles: application as antimicrobial and anticancer agent, Artificial Cells, Nanomedicine, and Biotechnology 46 (2018) 38–51, https://doi.org/10.1080/21691401.2018.1489262.
[66] Y.-Y. Dong, Y.-H. Zhu, M.-G. Ma, Q. Liu, W.-Q. He, Synthesis and characterization of Ag@AgCl-reinforced cellulose composites with enhanced antibacterial and photocatalytic degradation properties, Sci. Rep. 11 (2021) 3366, https://doi.org/10.1038/s41598-021-82447-2.
[67] K. Okaiyeto, M.O. Ojemaye, H. Hoppe, L.V. Mabinya, A.I. Okoh, Phytofabrication of silver/silver chloride nanoparticles using aqueous leaf extract of oedera genistifolia: characterization and antibacterial potential, Molecules 24 (2019) 4382, https://doi.org/10.3390/molecules24234382.
[68] K. Paulkumar, G. Gnanajobitha, M. Vanaja, S. Rajeshkumar, C. Malarkodi, K. Pandian, G. Annadurai, Piper nigrum leaf and stem assisted green synthesis of silver nanoparticles and evaluation of its antibacterial activity against agricultural plant pathogens, Sci. World J. 2014 (2014 Oct), https://doi.org/10.1155/2014/829894.
[69] S. Jebril, R. Khanfir Ben Jenana, C. Dridi, Green synthesis of silver nanoparticles using Melia azedarach leaf extract and their antifungal activities: in vitro and in vivo, Mater. Chem. Phys. 248 (2020) 122898, https://doi.org/10.1016/j.matchemphys.2020.122898.
[70] S.O. Aisida, K. Ugwu, P.A. Akpa, A.C. Nwanya, U. Nwankwo, S.S. Botha, P.M. Ejikeme, I. Ahmad, M. Maaza, F.I. Ezema, Biosynthesis of silver nanoparticles using bitter leave (Veronica amygdalina) for antibacterial activities, Surface. Interfac. 17 (2019) 100359, https://doi.org/10.1016/j.surfin.2019.100359.

[71] P. Das, K. Ghosal, N.K. Jana, A. Mukherjee, P. Basak, Green synthesis and characterization of silver nanoparticles using belladonna mother tincture and its efficacy as a potential antibacterial and anti-inflammatory agent, Mater. Chem. Phys. 228 (2019) 310–317, https://doi.org/10.1016/j.matchemphys.2019.02.064.
[72] R.F.N. Quadrado, G. Gohlke, R.S. Oliboni, A. Smaniotto, A.R. Fajardo, Hybrid hydrogels containing one-step biosynthesized silver nanoparticles: preparation, characterization and catalytic application, J. Ind. Eng. Chem. 79 (2019) 326–337, https://doi.org/10.1016/j.jiec.2019.07.008.
[73] J. Annamalai, T. Nallamuthu, Green synthesis of silver nanoparticles: characterization and determination of antibacterial potency, Appl. Nanosci. 6 (2016) 259–265, https://doi.org/10.1007/s13204-015-0426-6.
[74] A.S. Hassanien, A.A. Akl, A.H. Sáaedi, Synthesis, crystallography, microstructure, crystal defects, and morphology of $Bi_x Zn_{1-x} O$ nanoparticles prepared by sol–gel technique, CrystEngComm 20 (2018) 1716–1730, https://doi.org/10.1039/C7CE02173A.
[75] K.S. Almaary, S.R.M. Sayed, O.H. Abd-Elkader, T.M. Dawoud, N.F. El Orabi, A.M. Elgorban, Complete green synthesis of silver-nanoparticles applying seed-borne Penicillium duclauxii, Saudi J. Biol. Sci. 27 (2020) 1333–1339, https://doi.org/10.1016/j.sjbs.2019.12.022.
[76] S.S. Gandhad, P.R. Jeergal, E. Veena, L. Hublikar, L.D. Horakeri, S.N. Mathad, S.R. Patil, Synthesis and characterization of silver nanoparticles using green route, International Journal of Advanced Science and Engineering 8 (2022) 2252, https://doi.org/10.29294/IJASE.8.3.2022.2252-2259.
[77] MdH. Ali, MdA.K. Azad, K.A. Khan, MdO. Rahman, U. Chakma, A. Kumer, Analysis of crystallographic structures and properties of silver nanoparticles synthesized using PKL extract and nanoscale characterization techniques, ACS Omega 8 (2023) 28133–28142, https://doi.org/10.1021/acsomega.3c01261.
[78] J.M. Ashraf, M.A. Ansari, H.M. Khan, M.A. Alzohairy, I. Choi, Green synthesis of silver nanoparticles and characterization of their inhibitory effects on AGEs formation using biophysical techniques, Sci. Rep. 6 (2016) 20414, https://doi.org/10.1038/srep20414.
[79] N. Hashim, M. Paramasivam, J.S. Tan, D. Kernain, M.H. Hussin, N. Brosse, F. Gambier, P.B. Raja, Green mode synthesis of silver nanoparticles using Vitis vinifera's tannin and screening its antimicrobial activity/apoptotic potential versus cancer cells, Mater. Today Commun. 25 (2020) 101511, https://doi.org/10.1016/j.mtcomm.2020.101511.
[80] C. Li, D. Chen, H. Xiao, Green synthesis of silver nanoparticles using Pyrus betulifolia Bunge and their antibacterial and antioxidant activity, Mater. Today Commun. 26 (2021) 102108, https://doi.org/10.1016/j.mtcomm.2021.102108.
[81] J.A. García-Ramón, R. Carmona-García, M. Valera-Zaragoza, A. Aparicio-Saguilán, L.A. Bello-Pérez, A. Aguirre-Cruz, J. Alvarez-Ramirez, Morphological, barrier, and mechanical properties of banana starch films reinforced with cellulose nanoparticles from plantain rachis, Int. J. Biol. Macromol. 187 (2021) 35–42, https://doi.org/10.1016/j.ijbiomac.2021.07.112.
[82] P.A. Méndez, Á.M. Méndez, L.N. Martínez, B. Vargas, B.L. López, Cassava and banana starch modified with maleic anhydride-poly (ethylene glycol) methyl ether (Ma-mPEG): a comparative study of their physicochemical properties as coatings, Int. J. Biol. Macromol. 205 (2022) 1–14, https://doi.org/10.1016/j.ijbiomac.2022.02.053.
[83] A.A. Barzinjy, The importance of essential-oils in the green synthesis of silver nanoparticles, J. Kor. Chem. Soc. 66 (4) (2022 Aug) 284–297, https://doi.org/10.5012/jkcs.2022.66.4.284.
[84] S. Raj, S.C. Mali, R. Trivedi, Green synthesis and characterization of silver nanoparticles using Enicostemma axillare (Lam.) leaf extract, Biochem. Biophys. Res. Commun. 503 (4) (2018) 2814–2819, https://doi.org/10.1016/j.bbrc.2018.08.045.
[85] S. Singla, A. Jana, R. Thakur, C. Kumari, S. Goyal, J. Pradhan, Green synthesis of silver nanoparticles using Oxalis griffithii extract and assessing their antimicrobial activity, Open 7 (2022 Jul 1) 100047, https://doi.org/10.1016/j.onano.2022.100047.
[86] M. Ohiduzzaman, M.N.I. Khan, K.A. Khan, B. Paul, Biosynthesis of silver nanoparticles by banana pulp extract: characterizations, antibacterial activity, and bioelectricity generation, Heliyon 10 (2024) e25520, https://doi.org/10.1016/j.heliyon.2024.e25520.